MNRAS **455,** 2826–2838 (2016) doi:10.1093/mnras/stv2453

The SAMI Galaxy Survey: can we trust aperture corrections to predict star formation?

S. N. Richards,[1,2,3★] J. J. Bryant,[1,2,3] S. M. Croom,[1,3] A. M. Hopkins,[2] A. L. Schaefer,[1,2,3] J. Bland-Hawthorn,[1] J. T. Allen,[1,3] S. Brough,[2] G. Cecil,[1,4] L. Cortese,[5] L. M. R. Fogarty,[1,3] M. L. P. Gunawardhana,[6] M. Goodwin,[2] A. W. Green,[2] I.-T. Ho,[7,8] L. J. Kewley,[8] I. S. Konstantopoulos,[2,9] J. S. Lawrence,[2] N. P. F. Lorente,[2] A. M. Medling,[8] M. S. Owers,[2,10] R. Sharp,[3,8] S. M. Sweet[8] and E. N. Taylor[11]

[1] *Sydney Institute for Astronomy, School of Physics, University of Sydney, Sydney NSW 2006, Australia*
[2] *Australian Astronomical Observatory, PO Box 915, North Ryde NSW 1670, Australia*
[3] *CAASTRO: ARC Centre of Excellence for All-sky Astrophysics*
[4] *Department of Physics and Astronomy, University of North Carolina, Chapel Hill, NC 27510, USA*
[5] *International Centre for Radio Astronomy Research, University of Western Australia, 35 Stirling Hwy, Crawley WA 6009, Australia*
[6] *Institute for Computational Cosmology and Centre for Extragalactic Astronomy, Department of Physics, Durham University, South Road, Durham, DH1 3LE, UK*
[7] *Institute for Astronomy, University of Hawaii, 2680 Woodlawn Drive, Honolulu, HI 96822, USA*
[8] *Research School of Astronomy and Astrophysics, Australian National University, Cotter Rd., Weston ACT 2611, Australia*
[9] *Envizi, Level 2, National Innovation Centre, Australian Technology Park, 4 Cornwallis Street, Eveleigh NSW 2015, Australia*
[10] *Department of Physics and Astronomy, Macquarie University, Sydney NSW 2109, Australia*
[11] *School of Physics, The University of Melbourne, Parkville VIC 3010, Australia*

Accepted 2015 October 19. Received 2015 October 19; in original form 2015 August 26

ABSTRACT

In the low-redshift Universe ($z < 0.3$), our view of galaxy evolution is primarily based on fibre optic spectroscopy surveys. Elaborate methods have been developed to address aperture effects when fixed aperture sizes only probe the inner regions for galaxies of ever decreasing redshift or increasing physical size. These aperture corrections rely on assumptions about the physical properties of galaxies. The adequacy of these aperture corrections can be tested with integral-field spectroscopic data. We use integral-field spectra drawn from 1212 galaxies observed as part of the SAMI Galaxy Survey to investigate the validity of two aperture correction methods that attempt to estimate a galaxy's total instantaneous star formation rate. We show that biases arise when assuming that instantaneous star formation is traced by broad-band imaging, and when the aperture correction is built only from spectra of the nuclear region of galaxies. These biases may be significant depending on the selection criteria of a survey sample. Understanding the sensitivities of these aperture corrections is essential for correct handling of systematic errors in galaxy evolution studies.

Key words: techniques: spectroscopic – galaxies: evolution.

1 INTRODUCTION

Over the past decade, aperture correction methods have been developed to obtain global properties of galaxies by extrapolating measurements from a single spectrum probing only the central regions of each galaxy. When a nearby galaxy is spectroscopically observed with a single aperture, such as an optical fibre with a diameter on-sky of a few arcseconds, only the central region of a galaxy is typically probed for redshifts $z \lesssim 0.3$. The magnitude of an aperture effect scales with both redshift and the physical size of a galaxy.

The largest single aperture galaxy surveys to date are the Sloan Digital Sky Survey (SDSS[1]; York et al. 2000) and the Galaxy And Mass Assembly survey (GAMA[2]; Driver et al. 2009). Both are

★ E-mail: samuel@physics.usyd.edu.au

[1] http://www.sdss3.org/
[2] http://www.gama-survey.org/

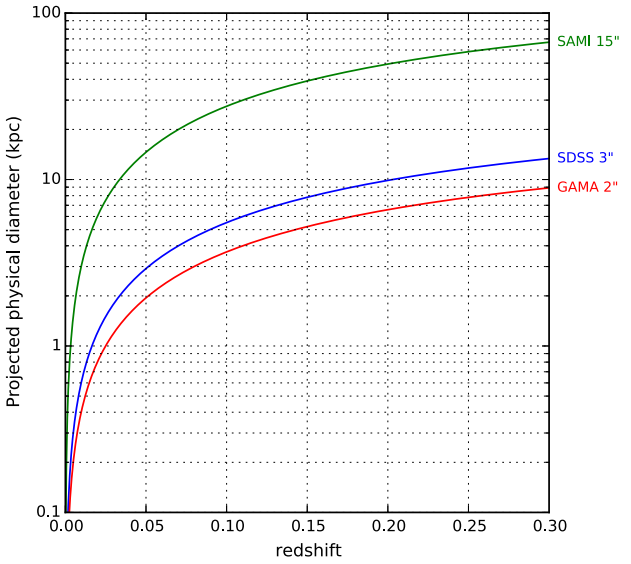

Figure 1. The projected physical sizes of the GAMA (2 arcsec, red), SDSS (3 arcsec, blue) and SAMI (15 arcsec, green) apertures as a function of redshift. For galaxies with redshift $z \lesssim 0.2$, only the central few kpc are observed spectrally in GAMA and SDSS.

optical spectroscopic surveys of $\approx 10^5$–10^6 nearby galaxies with $z \lesssim 0.3$, and have on-sky fibre diameters of 3 and 2 arcsec, respectively. Therefore, the star formation rate (SFR) of galaxies within these surveys are subject to aperture effects. Fig. 1 shows the equivalent physical scale of an aperture's on-sky diameter as a function of redshift. By design however, GAMA incorporates spectra from other sources, including SDSS for bright galaxies.

The SFR aperture correction used in GAMA and SDSS is different, with GAMA using a method prescribed by Hopkins et al. (2003, hereafter H03), and SDSS that presented by Brinchmann et al. (2004, hereafter B04). For the benefit of the reader, a short summary of each method is provided.

1.1 Hopkins et al. (2003) method (H03, GAMA)

In a detailed look at SFR indicators from multiwavelength data (1.4 GHz to u-band luminosities), H03 found that multiplying the stellar absorption corrected Hα equivalent width, EW(Hα), from the fibre spectrum by the galaxy's k-corrected Petrosian r-band luminosity, and correcting for the Balmer decrement, gave a good approximation to the galaxy's total SFR, given by

$$\mathrm{SFR\,(H03)} = \frac{\mathrm{EW(H\,\alpha)} \times 10^{-0.4(M_r - 34.10)}}{\mathrm{SFRF}} \times \frac{3 \times 10^{18}}{[6564.61\,(1+z)]^2} \cdot \left(\frac{\mathrm{BD}}{2.86}\right)^{2.36}, \quad (1)$$

where EW(Hα) is the stellar absorption corrected Hα flux divided by the median continuum level of the spectrum about the Hα emission line (we perform the absorption correction by subtracting fitted stellar templates via LZIFU), M_r is the absolute k-corrected r-band Petrosian magnitude of the galaxy including a correction for Galactic extinction, z is the flow-corrected redshift of the galaxy and BD is the Balmer decrement (stellar absorption corrected ratio of Hα/ Hβ emission-line fluxes) assuming a fixed Case-B recombination value of 2.86 (Calzetti 2001; Dopita & Sutherland 2003) with a reddening slope of 2.36 (Cardelli, Clayton & Mathis 1989) and the dust as a foreground screen averaged over the galaxy. SFRF is the "SFR factor" to convert to solar masses per year, e. g. 1.27×10^{34} W, as given by Kennicutt (1998) assuming a Salpeter (1955) initial mass function (IMF).

Only galaxies classified as star forming (SF) via the Kauffmann et al. (2003) limit in Baldwin, Phillips & Terlevich (1981, hereafter BPT) diagnostics were considered in this aperture correction. It assumes that the galaxy's EW(Hα) and Balmer decrement profiles are constant across the galaxy. For the current work, we interpret this to mean that for an EW(Hα) measured using different aperture radii, to the limit of 2 Petrosian radii (hereafter R_{2P}), the H03 SFR derived in those apertures will be constant.

Due to the straightforward approach of this aperture correction, H03 have been widely used in determining the SFR of galaxies in single aperture surveys. In the absence of large integral-field surveys, no formal error analysis of the assumptions in H03 has been possible. Consequently, no errors on the SFRs are provided in GAMA DR2 (Liske et al. 2015). What has been examined is how well the H03 SFRs compare with SFRs derived from other indicators (H03; Cluver et al. 2014, Wang et al., in preparation). The limit of these studies lies in how to interpret the random and systematic errors due to different indicators tracing different star formation time-scales.

1.2 Brinchmann et al. (2004) method (B04, SDSS)

Younger, hotter stars (that contribute most of the star formation component of Hα emission) are observed to have bluer optical colours, so B04 included a three-colour dependence in their aperture correction (using the SDSS filters g, r, i at a rest frame of $z = 0.1$). The best way to think about the B04 aperture correction is not as an aperture correction equation, but rather an aperture correction cube. The x, y-axes are the $g - r$, $r - i$ colours, and the z-axis a histogram (likelihood distribution) of the SFR divided by the i-band luminosity (a proxy for specific-SFR) for each galaxy in a given $g - r$, $r - i$ cell. B04 constructed this aperture correction cube using spectra from high signal-to-noise (s/n) SF galaxies in SDSS, with the g, r, i colours and Hα-based SFR coming from within the fibre.

Using this aperture correction cube, it is then possible to find the likelihood distribution of SFR when only optical colours are known (independent of aperture size or shape). To calculate the B04 SFR: (a) measure the Hα SFR from within the fibre; (b) subtract the g, r, i fibre flux from the g, r, i total galaxy flux to find the g, r, i colours of the galaxy's light outside of the fibre aperture (annulus magnitudes); (c) locate the cell where the colours of the annulus magnitudes lie on the aperture correction cube's $g - r$, $r - i$ grid; (d) multiply the likelihood distribution of the located cell by the annulus' i-band luminosity to find the SFR likelihood distribution of the annulus; (e) calculate the B04 SFR by adding together the SFR measured in the fibre and the median SFR from the SFR likelihood distribution of the annulus. It is worth clarifying that the B04 method of predicting the SFR of the annulus is independent from the aperture (fibre).

There are three main assumptions in B04's original approach to calculating the SFR for SDSS galaxies. The first assumption relates to the method of calculating the fibre SFR for all galaxy types (defined as SF, low-s/n SF, AGN/composites from BPT diagnostics). For SF galaxies, the emission lines, predominantly Hα, were used to find the fibre SFR by fitting models to the spectra (Charlot & Longhetti 2001). For other galaxy types, the fibre SFR was found by using a relationship of specific-SFR to D4000 (so as to not be biased by non-SF contributions to the emission lines). This relationship was constructed using spectra from SF galaxies. In a detailed look at this assumption, Salim et al. (2007, using UV-based SFRs) found

that non-SF galaxies followed different relationships depending on their BPT classification. As such, B04 revised this relationship in more recent editions of their SDSS SFRs. This particular revision only applies to classifications other than SF galaxies, though all B04 SFRs are adjusted[3] in later editions due to improvements in the SDSS data reduction pipeline and model fitting the photometry of the outer regions of each galaxy.

The second assumption, which is more directly related to the aperture correction cube, is that optical colours are a good indicator of the Hα specific-SFR. The most obvious possible discrepancy is that the stellar continuum and Hα emission vary on two different time-scales ($\approx$100 and 10 Myr, respectively). B04 assume the uncertainties are not systematic and provided them as percentile ranges of the likelihood distributions. Salim et al. (2007) quote average 1σ errors on B04 SFRs in the range of 0.29–0.54 dex depending on the BPT classification. The aperture correction cube has a degeneracy between stellar age, metallicity and dust, which is assumed to broaden the likelihood distribution for any given $g-r$, $r-i$ cell.

The third assumption is that the 3-colour relationship with SFR in the nucleus of a galaxy is the same for that of the disc. Constructing the aperture correction cube with only nuclear spectra could lead to regions on the $g-r$, $r-i$ grid that are biased, in particular for galaxies with redshift, $z < 0.1$, and so lead to systematic errors in SFR.

1.3 Previous tests of H03 and B04 SFRs

Slit-scanning data from the Nearby Field Galaxy Survey (NFGS; Jansen et al. 2000a,b) were used by Kewley, Jansen & Geller (2005) to look at the biases of aperture effects on SFR, metallicity and reddening. They found that if a single aperture (fibre) could capture >20 per cent of the galaxy's light, the systematic and random errors from the aperture effects would be minimized, but if <20 per cent then the aperture effects are substantial. This 20 per cent boundary corresponds to redshifts of 0.04 and 0.06 for SDSS and GAMA, respectively.

Data obtained via integral-field spectroscopy (IFS) is the preferred method for testing aperture corrections, due to the data being spatially resolved. It enables spectroscopic comparisons of the nuclear region, the disc, and the integrated light. Studies of galaxies observed via IFS that look at the effect of aperture corrections include Gerssen, Wilman & Christensen (2012), Iglesias-Páramo et al. (2013) and Brough et al. (2013). Iglesias-Páramo et al. (2013) use the data of 104 SF galaxies from the Calar Alto Legacy Integral Field Area Survey (CALIFA; Sánchez et al. 2012) to measure the curves of growth of the Hα flux, Balmer decrement and EW(Hα), and empirically find aperture corrections as a function of r_a/R_{50}, where r_a is the radius of a single aperture and R_{50} the half-light radius (the radius containing 50 per cent of the Petrosian flux in the r band). Gerssen et al. (2012) compare the B04 aperture corrections with a sample of 24 SF galaxies observed with VIMOS (Le Fèvre et al. 2003). They compared the ratio of the B04 aperture-corrected SFR to the fibre SFR with the ratio of the total Hα flux to the Hα flux contained within a 3 arcsec aperture on their data cubes. They find on average for their sample that the B04 correction underestimates the aperture correction factor by a factor $\approx$2.5 with a large scatter. Brough et al. (2013) directly compare H03 and B04 SFRs with SFRs from IFS data of 18 galaxies that span a range of environments, as observed with SPIRAL (Sharp et al. 2006). They find a mean ratio of 1.26 $\pm$ 0.23 and 1.34 $\pm$ 0.17 respective to H03 and B04.

Although several studies compare the H03 and B04 SFRs of galaxies with SFRs from total Hα, all are limited by errors from either small-sample statistics or the inability to disentangle measurement and calibration biases (Calzetti & Kennicutt 2009).

Until recently, nearly all IFS data have been obtained with monolithic IFUs, meaning that the time taken to gather the data has been lengthy and the sample numbers small ($\lesssim$100, normally a few dozen). Efforts have now been made towards obtaining IFS data of $>10^3$ galaxies with multi-object IFS, improving an IFS survey speed by over an order of magnitude on monolithic IFUs. Such instruments include the Sydney-AAO Multi-object Integral-field spectrograph (SAMI[4]; Croom et al. 2012; Bryant et al. 2015), Mapping Nearby Galaxies at APO Instrument (MaNGA[5]; Bundy et al. 2015; Drory et al. 2015) and the K-band Multi-Object Spectrograph (KMOS[6]; Sharples et al. 2006, 2013).

For this work, we use data obtained as part of the SAMI Galaxy Survey (Allen et al. 2015; Bryant et al. 2015; Sharp et al. 2015), which already has reduced IFS data on 1212 galaxies at the time of writing, with a survey target sample of 3400 over 3 yr. With a large initial sample, the SAMI Galaxy Survey makes for an ideal data set to test the robustness of the H03 and B04 aperture corrections methods.

In Section 2, we detail the observations and data reduction of the SAMI Galaxy Survey, the sample selection and cuts applied to the SAMI Galaxy Survey data, and the ancillary data of the SAMI Galaxy Survey important to this work. In Section 3, we perform tests of the H03 and B04 aperture corrections both indirectly and directly. In Section 4, we discuss biases of the H03 and B04 methods and implications these might have on literature results. In Section 5, we conclude on the trustworthiness of the H03 and B04 aperture corrections and provide advice for future single aperture studies. Throughout this paper, 'SF' is in reference to galaxies or spectra that lie below the Kauffmann et al. (2003) star formation line on the $\log_{10}$([O III] λ5007/Hβ) versus $\log_{10}$([N II] λ6583/Hα) BPT diagram. We assume the standard Λ cold dark matter cosmology with $\Omega_m = 0.3$, $\Omega_\Lambda = 0.7$ and $H_0 = 70$ km s^{-1} Mpc^{-1}.

2 OBSERVATIONS AND DATA REDUCTION

The data used in this work were obtained with SAMI, which deploys 13 hexabundles (Bland-Hawthorn et al. 2011; Bryant et al. 2014) over a 1° field at the Prime Focus of the 3.9 m Anglo-Australian Telescope. Each hexabundle consists of 61 circularly packed optical fibres. The core size of each fibre is 1.6 arcsec, giving each hexabundle a field of view of 15 arcsec diameter. All 819 fibres (793 object fibres and 26 sky fibres) feed into the AAOmega spectrograph (Sharp et al. 2006). For SAMI observing, AAOmega is configured to a wavelength coverage of 370–570 nm with $R = 1730$ in the blue arm, and 625–735 nm with $R = 4500$ in the red arm. A seven point dither pattern achieves near-uniform spatial coverage (Sharp et al. 2015), with 1800 s exposure time for each frame, totalling 3.5 h per field.

As described in Allen et al. (2015), in every field, 12 galaxies and a secondary standard star are observed. The secondary standard

[3] http://wwwmpa.mpa-garching.mpg.de/SDSS/DR7/

[4] SAMI: http://sami-survey.org/

[5] MaNGA: http://www.sdss3.org/future/manga.php

[6] KMOS: http://www.eso.org/sci/facilities/develop/instruments/kmos.html

star is used to probe the conditions as observed by the entire instrument. The flux zero-point is obtained from primary standard stars observed in a single hexabundle during the same night for any given field of observation. The raw data from SAMI were reduced using the AAOmega data reduction pipeline, 2dfDR,[7] followed by full alignment and flux calibration through the SAMI Data Reduction pipeline (see Sharp et al. 2015 for a detailed explanation of this package). In addition to the reduction pipeline described by Allen et al. (2015) and Sharp et al. (2015), the individual frames are now scaled to account for variations in observing conditions. Absolute *g*-band flux calibration with respect to SDSS imaging across the survey is unity with a 9 per cent scatter, found by taking the ratio of the summed flux within a 12 arcsec diameter aperture centred on the galaxy in a *g*-band SAMI IFU image and the respective SDSS *g*-band image smoothed to the SAMI seeing.

Emission-line maps (most notably Hβ, [O III] λ5007, Hα and [N II] λ6583) of all galaxies in the SAMI Galaxy Survey were produced using the IFU emission-line fitting package, LZIFU (see Ho et al. (2014) for a detailed explanation of this package). LZIFU utilizes pPXF (Cappellari & Emsellem 2004) for stellar template fitting (MILES templates; Falcón-Barroso et al. 2011) and the MPFIT library (Markwardt 2009) for estimating emission-line properties. It is possible to perform multicomponent fitting to each emission line with LZIFU, although for the purpose of this work we chose to only use the single-component Gaussian fits.

2.1 Sample selection

At the time of writing, 1212 galaxies had been observed as part of the SAMI Galaxy Survey (internal data release v0.9), and form the parent sample for the analysis in this work. The SAMI Galaxy Survey can be split into two populations of galaxies: those found in the GAMA regions (field galaxies) and those found in the Cluster regions (cluster galaxies). For a full description of the SAMI Galaxy Survey target selection, we refer the reader to Bryant et al. (2015). Of the 1212 galaxies in our parent sample, 832 are found in the GAMA regions and 380 in the Cluster regions. Fig. 2 shows the stellar mass of these galaxies as a function of redshift, and reveals that the distribution of our parent sample is representative of the full SAMI Galaxy Survey's target selection. Different aspects of the analysis in this work use different subsamples of this parent sample, which are defined at the start of each section, respectively.

2.2 Ancillary data

The target selection of the SAMI Galaxy Survey (Bryant et al. 2015) allows for a plethora of existing multiwavelength ancillary data, in particular for galaxies observed within the GAMA Survey fields (2/3 of the SAMI Galaxy Survey targets). Among many other properties, the GAMA DR2 catalogue (Liske et al. 2015) provides the Petrosian radii, stellar masses (Taylor et al. 2011), Sérsic fits with R_e measurements (Kelvin et al. 2012), and spectroscopic redshifts and H03 aperture-corrected SFRs (Hopkins et al. 2013; Gunawardhana et al. 2013) for every galaxy used in the analysis of this paper. Optical *u*, *g*, *r*, *i*, *z* photometry is provided by SDSS DR10 (Ahn et al. 2014), with the B04 total SFRs coming from the latest MPA-JHU Catalogue.[8] All stellar masses were found using the photometric prescription of Taylor et al. (2011). Following the scheme used by Kelvin et al. (2014) and Cortese et al. (2014), visual morphological classification has been performed on the SDSS colour images by the SAMI Galaxy Survey team. Galaxies were divided into late and early types (or unclassified) according to their shape, presence of spiral arms and/or signs of star formation.

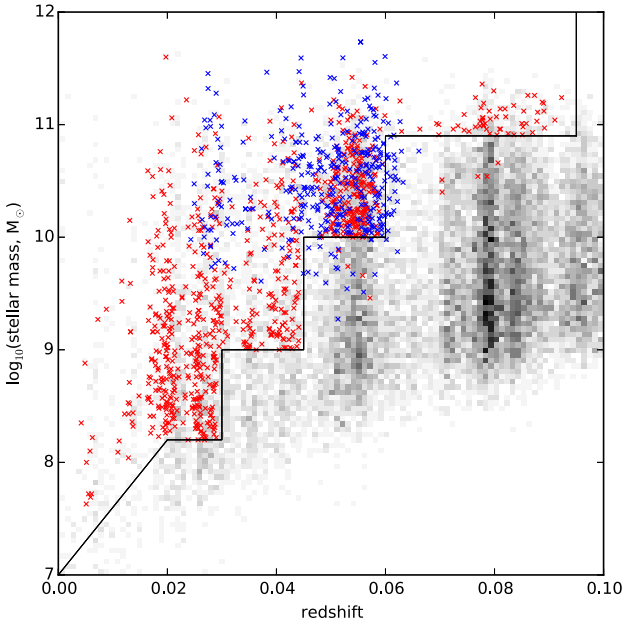

Figure 2. The location of our galaxies (red and blue points) overlaid on the SAMI Galaxy Survey target selection (see fig. 4 of Bryant et al. 2015). The red points are galaxies found in the GAMA regions, and the blue points those found in the Cluster regions. The background is a 2D histogram of the GAMA DR2 catalogue from which the SAMI field sample is drawn, with the black stepped line representing the selection cut. Galaxies above this line are 'Primary Targets'. Galaxies that lie below this line are considered 'Filler Targets' (included due to observational constraints on field tiling). Our sample of 1212 galaxies is representative of the full SAMI target selection.

3 TESTING OF APERTURE CORRECTIONS

In this section, we aim to provide analysis of the H03 and B04 aperture corrections using integral-field data from the SAMI Galaxy Survey. The analysis is divided into three sections, with the first being the comparison of SFRs from the H03 and B04 methods to that measured from SAMI galaxies, and the second and third being investigations into the assumptions of the H03 and B04 method, respectively.

3.1 Comparing total SFRs from SAMI, GAMA and SDSS

The most common test of aperture corrections is in the comparison of the total Hα SFRs measured from IFS data to that from an aperture correction. IFS data provide direct knowledge of the total instantaneous SFR of a galaxy (when full coverage is obtained),

[7] 2dfDR is a public data reduction package managed by the Australian Astronomical Observatory, see http://www.aao.gov.au/science/software/2dfdr.

[8] B04 total SFRs are found in 'gal_totsfr_dr7_v5_2.fits.gz', obtained at http://www.mpa-garching.mpg.de/SDSS/DR7/sfrs.html. The SFRs are derived from SDSS DR7 data (Abazajian et al. 2009), and include the corrections of Salim et al. (2007).

whereas the aperture corrections are predicting the total SFR indirectly. To do this comparison, from the 1212 parent sample we selected galaxies that met the following criteria: (1) matched to, and had measured SFRs in the GAMA and SDSS catalogues; (2) classified as SF from the integrated SAMI spectrum via the Kauffmann et al. (2003) limit in BPT diagnostics; (3) the SAMI hexabundle field of view probes out to at least 2 effective radii ($2R_e$). After these cuts, we were left with 107 galaxies. The SAMI SFRs were measured by binning the SAMI data cube, taking into account the spatial covariance (Sharp et al. 2015) and fitting the binned spectrum with LZIFU. The single-component emission-line fits of the LZIFU product were then used to compute the SFR via:

$$\mathrm{SFR\,(SAMI)} = \frac{\mathrm{H}_\alpha \cdot \left(4 \cdot \pi \cdot {d_l}^2\right)}{\mathrm{SFRF}} \cdot \left(\frac{\mathrm{BD}}{2.86}\right)^{2.36}, \quad (2)$$

where Hα is the integrated flux (in W m^{-2}) of the single-component Gaussian fit of the Hα emission line after stellar continuum subtraction; SFRF is the SFR factor to convert to solar masses per year $= 1.27\times 10^{34}$ W, as given by Kennicutt (1998) assuming a Salpeter (1955) IMF and solar metallicity; d_l is the luminosity distance in metres; BD is the Balmer decrement (as described in equation (1) along with the reddening equation). We also ensure both H03 and B04 SFRs are scaled accordingly to match our use of a Salpeter (1955) IMF.

Fig. 3 shows the comparison between the SAMI SFRs and SFRs from H03 and B04, and suggests there are slight trends with respect to the SAMI values in the H03 and B04 methods potentially biasing literature results that rely on them. Assuming the SAMI SFR to be the true SFR, the H03 method shows only overestimation for galaxies with a low SFR, whereas the B04 show both over- and underestimation for low- and high-SFR galaxies, respectively. H03 exhibit a larger scatter than B04 with scatters of 0.22 and 0.15 dex, respectively. The best fits to these data for each aperture correction are given as

$$\mathrm{SFR\,(SAMI)} = \frac{\mathrm{SFR\,(H03)} - (0.02 \pm 0.04)}{(0.91 \pm 0.05)}, \quad (3)$$

$$\mathrm{SFR\,(SAMI)} = \frac{\mathrm{SFR\,(B04)} + (0.09 \pm 0.02)}{(0.85 \pm 0.03)}, \quad (4)$$

where all SFRs are in $\log_{10}(\mathrm{M}_\odot\ \mathrm{yr}^{-1})$. After visually noticing a gradient in stellar mass in Fig. 3(d), we found no significant gain when including a stellar mass term for the B04 fit.

Comparing SFRs can reveal the presence of systematic errors, but as with all analysis of aperture corrections performed with this technique it is not possible to locate the origin of such errors from the SFRs alone. To locate biases in aperture corrections, rather than comparing SFRs from different methods, tests should be performed on the assumptions that go into the aperture corrections.

3.2 Testing the H03 aperture correction with SAMI data

With IFS data it is possible to directly test the assumptions of H03 that a galaxy's EW(Hα) and Balmer decrement profiles are flat. The form of equation (1) means that for a galaxy observed with ever-increasing aperture sizes, the H03 SFR derived from the measured EW(Hα) and Balmer decrement in those apertures should remain constant. If the EW(Hα) and Balmer decrement profiles vary across a galaxy, the H03 SFR equated at ever-increasing aperture sizes should approach to the true total SFR when the aperture radius is equal to 2 × the galaxy's r-band Petrosian radius (R_{2P}).

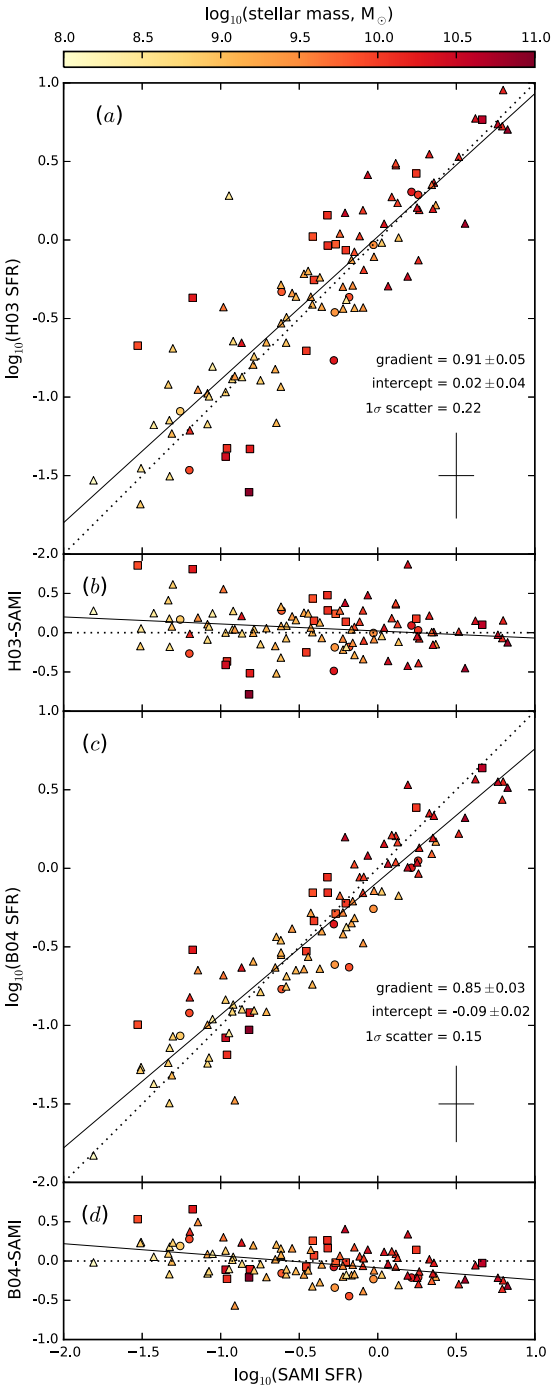

Figure 3. $\log_{10}$(SFR) in $\mathrm{M}_\odot\ \mathrm{yr}^{-1}$ of star-forming galaxies found by the methods (a) of Hopkins et al. (2003, H03) and SAMI, and (c) Brinchmann et al. (2004, B04) and SAMI. (b) and (d) show the residuals from a 1:1 correlation in (a) and (c), respectively. There are the same 107 data points (galaxies) in all diagrams, with their colours representing the $\log_{10}$(stellar mass, $\mathrm{M}_\odot$). Square, triangle and circle markers represent early-type, late-type and unclassified morphologies, respectively. The typical error bars for these data are given in the lower right of (a) and (c). No formal error for the H03 SFR is given GAMA DR2, so a typical error of the H03 method was taken from Hopkins et al. (2003). The dotted lines are lines of the unity relation. The solid lines are least-squares fits to these data with the gradient, intercept and 1σ scatter about the fit shown in the lower right of (a) and (c). These data span approximately 4 orders of magnitude in SFR from 0.01 to 10 $\mathrm{M}_\odot\ \mathrm{yr}^{-1}$.

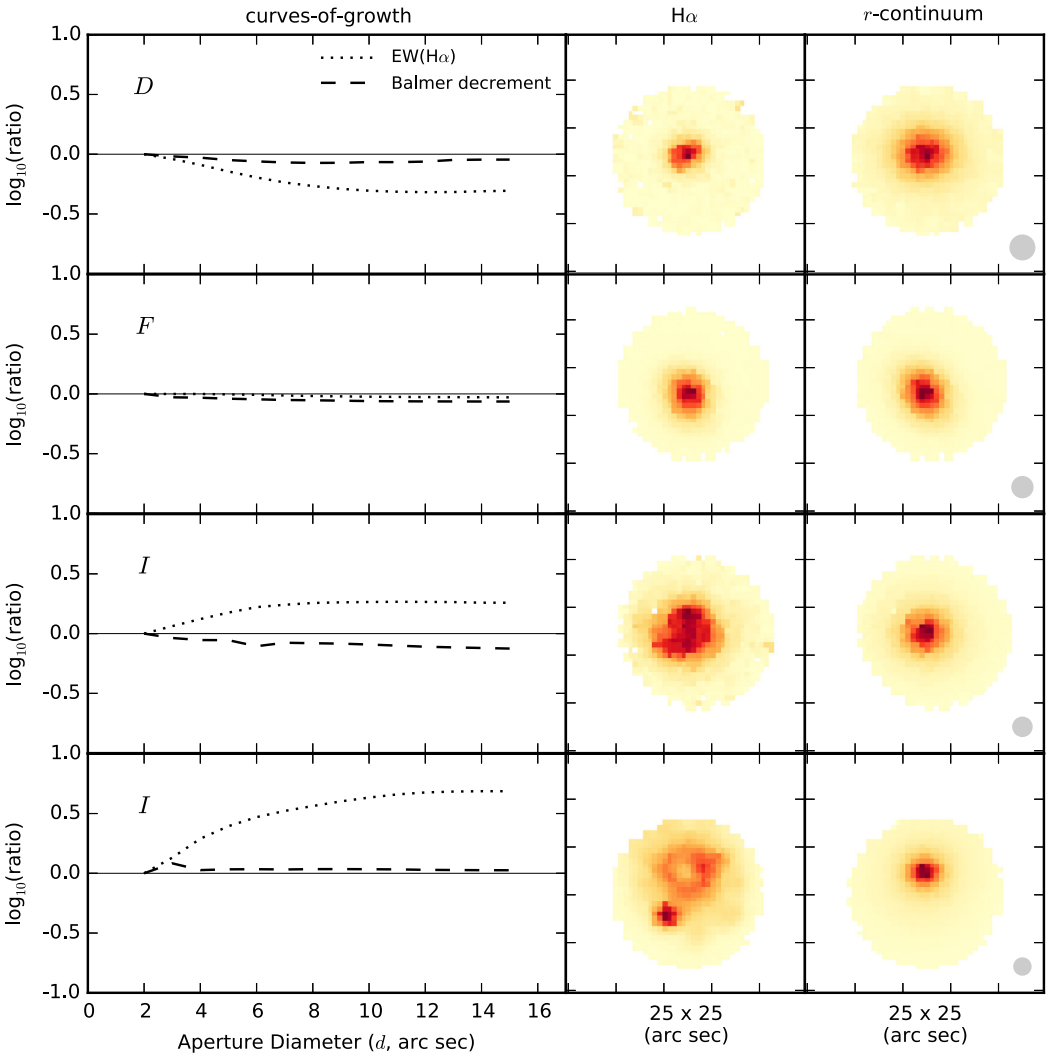

Figure 4. Example galaxies that fall within the respective curve of growth classifications: decreasing (*D*), flat (*F*) or increasing (*I*), where each row is a different galaxy. The first column shows the EW(Hα) and Balmer decrement curves of growth (dotted and dashed line, respectively). The curves of growth have been normalized to the measurement obtained with an aperture diameter of 2 arcsec ('ratio'). The second and third columns are the SAMI Hα and *r*-continuum maps for each galaxy (normalized to the maximum of each map for visual aid), and the size of the *g*-band PSF is given as a grey circle in the lower right of the *r*-continuum maps. All maps are 25 $\times$ 25 arcsec in size, and are orientated such that north is up and east is left. The Balmer decrement curves of growth tend to remain flat for all aperture sizes, but the EW(Hα) varies greatly depending on the relative distributions of Hα to *r*-continuum.

Equation (1) relies on three spectral measures: redshift, EW(Hα) and Balmer decrement. The first step in this test was to see how the latter two vary for apertures of d from 2 to 15 arcsec with a step of 1 arcsec for all SF galaxies in the 1212 parent sample that had an Hα s/n >3 for all apertures (leaving 461 galaxies). Galaxies that were excluded due to this cut had either AGN/LINER emission or no reliable Hα flux measurement in the smallest apertures. All galaxies that exhibited extra-nuclear star formation still had detectable Hα flux in the smallest apertures. The spectrum for each aperture was obtained by binning all spaxels of the SAMI data cube (taking into account spatial covariance) that fell within the aperture footprint centred on the galaxy. The EW(Hα) and Balmer decrement for each spectrum were found by fitting each spectrum with LZIFU. The data for each galaxy were then normalized by its respective measurement at $d = 2$, resulting in a curve of growth of each galaxy's EW(Hα) and Balmer decrement (see leftmost column of Fig. 4).

Overall, the Balmer decrement curves of growth tend to be flat for all galaxy types (staying within a range of 0.1 dex), but the EW(Hα) curves of growth vary greatly (in extreme cases there can be more than an order of magnitude difference between $d = 2$ and $d = 15$). The EW(Hα) curves of growth can be categorized as either decreasing (155 galaxies), flat (149 galaxies) or increasing (157 galaxies). The classifications were performed by allowing the flat (*F*) curves of growth to have a range of $\pm$0.05 dex between $d = 2$ and $d = 15$. Higher and lower than this range, the curves of growth were classified as increasing (*I*) and decreasing (*D*), respectively.

Fig. 4 provides example galaxies for each classification, and it immediately becomes evident as to why the EW(Hα) curves of growth vary so much when inspecting the Hα and *r*-continuum maps (middle and rightmost columns). *D* have more centrally concentrated Hα compared to their *r*-continuum, *F* have similar Hα and *r*-continuum profiles, and *I* fall into two subcategories: either the *r*-continuum shows a steeper radial decrease than the Hα emission,

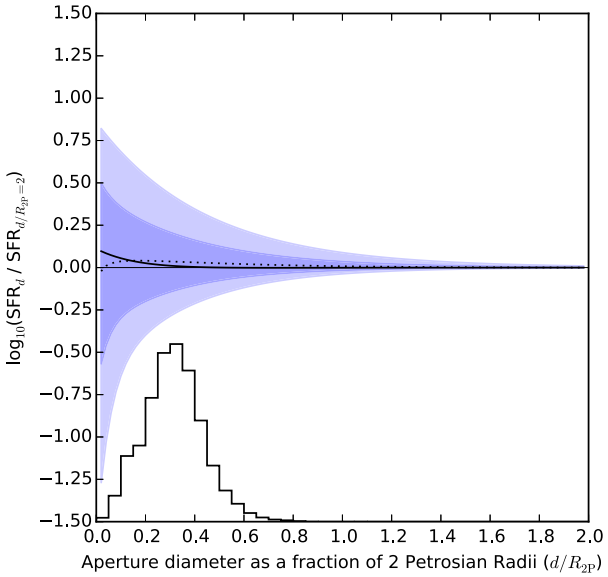

Figure 5. The error distribution of an H03 derived SFR as a function of aperture size. The percentile ranges for all 461 H03 curves of growth are shown as shaded regions, and their curve-of-growth lines from the bottom-up are 2.5, 16, 50 (median; thick line), 84 and 97.5 per cent. The dotted line is the curve of growth of the mean. The thin horizontal line is unity. The y-axis is $\log_{10}(\mathrm{SFR}_d$ / $\mathrm{SFR}_{d/R_{2P}=2})$. The equations and coefficients of the fits to the percentiles can be found in Table 1. The stepped-histogram shows the distribution of respective aperture sizes for all GAMA DR2 galaxies with redshift $z < 0.1$, only including those measured with a 2 arcsec aperture. This means that for a galaxy whose $d/R_{2P} = 0.3$, the 1σ error on its H03 SFR is 0.18 dex. For the smallest aperture sizes (i.e. large, nearby galaxies), the 1σ error becomes ∼0.5 dex, and the median departs from unity to become ∼0.1 dex, meaning H03 is more likely to overestimate the SFR by ∼0.1 dex. This error is only due to aperture effects. To get the full uncertainty of SFR, random and systematic errors on the flux, modelling, initial mass function, etc. would need be been taken into account.

or there are off-centred SF regions (bright in Hα) that don't show up in the r-continuum. The H03 aperture correction (equation 1) relies on the EW(Hα) and Balmer decrement curves of growth being flat, which this analysis shows is only true 1/3 of the time.

To quantify the error of this assumption, we find the H03 SFR curve of growth for each galaxy over the same aperture range, and fit each curve of growth with an exponential, constrained such that the exponential has to reach within 1 per cent of its asymptote at $d/R_{2P} = 2$ (by definition of equation 1). A H03 SFR curve of growth can be fitted with an exponential such that the residual on the fit is typically less than 0.05 dex for all apertures. To put all the H03 curves of growth on the same diagram, we normalized each fit by the SFR found at $d/R_{2P} = 2$, and converted the aperture sizes to units of d/R_{2P}. Combining the curves of growth like this enables us to measure the percentile ranges for different aperture sizes. A diagram of these percentiles can be found in Fig. 5, which includes the H03 curves of growth from 461 galaxies. The shape of the percentiles can be fitted with the analytical expression:

$$\log_{10}(\text{error}) = A \cdot \exp\left(B \cdot \frac{d}{R_{2P}}\right) + C \cdot \exp\left(D \cdot \frac{d}{R_{2P}}\right), \qquad (5)$$

where error is the percentile error on the H03 aperture-corrected SFR; A, B, C and D are the coefficients given in 1 respective to their percentile; d is the size of the aperture diameter in arcsec; R_{2P} is the $2 \times r$-band Petrosian radius of the galaxy in arcsec. This analytical expression can be used to find the percentile error distribution on the H03 SFR for any given galaxy. For redshifts $z < 0.1$, a GAMA DR2 galaxy has a median $d/R_{2P} \approx 0.3$, resulting in a 1σ error on its H03 SFR of 0.18 dex. This error is only the error on the assumptions that go into the H03 aperture correction, and to get formal errors, the EW(Hα) and Balmer decrement measurement errors would have to be included. We found no correlation between a galaxy's H03 SFR curve of growth and a global property of the galaxy (including: SFR at $d/R_{2P} = 2$, stellar mass, r-band Sérsic index, Petrosian $g - r$ colour, redshift and 5th Nearest Neighbour environment density).

Table 1. Table of coefficients to find the errors for a galaxy's SFR after it has undergone the H03 aperture correction (see Fig. 5 for a description of these fits). Equation (5) is to be used for calculating the percentiles. The 'resid' column shows the median residual of the fit in dex for the range $0.01 < d/R_{2P} < 1.00$. The median (50th percentile) can be considered as an adjustment to the H03 SFRs. We do not presume to know the significance of the fitting coefficients to five decimal places, but they are provided for the sake of computation.

Percentile	A	B	C	D	resid
2.5	−0.926(18)	−19.637(70)	−0.682(22)	−2.919(96)	0.013
16.0	−0.369(69)	−3.129(41)	−0.365(93)	−25.097(86)	0.004
50.0	−5.606(92)	−4.807(18)	5.717(52)	−4.844(72)	0.003
84.0	0.442(29)	−2.503(26)	0.118(49)	−20.431(52)	0.005
97.5	0.432(06)	−2.274(50)	0.426(35)	−2.274(49)	0.014

3.3 Testing the B04 aperture correction with SAMI data

There are two assumptions that go into the B04 aperture correction cube that we can examine: (1) broad-band optical colours can act as a tracer of the Hα-based SFR; (2) an aperture correction cube created from spectra probing only the nuclear regions of galaxies can be representative of a galaxy's disc. The widths of the SFR likelihood distributions that come from the aperture correction cube are representative of the errors due to the first assumption. B04 provide the percentiles of the SFR likelihood distributions of each galaxy. Obtaining a formal error on the second assumption from this analysis is not possible due to mismatching of available data between SAMI and B04, which will become clear as the analysis progresses.

To examine the assumption that broad-band optical colours can act as a tracer of the SFR(Hα), we first need to construct a SAMI version of the aperture correction cube (hereafter ACC). In B04, the SDSS optical filters g, r, i are used to construct their aperture correction cube, but the wavelength range of SAMI does not span that entire filter set. Instead, we opt to use a custom top-hat filter set that can be applied to the spectra (k-corrected to $z = 0$), taking the notation u^s, g^s, r^s as they most closely match the standard u, g, r filters, respectively (see Fig. 6). The adoption of a custom filter set means that the magnitude of any bias or relation found with our data is not representative of the B04 aperture correction cube. The presence of a bias or relation, however, would indicate that one would likely also be present in the B04 aperture correction cube.

The native spaxel (spatial pixel) size of the SAMI data cubes is 0.5 arcsec square, though to improve s/n, especially in the outer discs of galaxies, we opted to bin the data such that the spaxel size is now 1 arcsec square. Taking all SF spaxels, we computed their u^s, g^s, r^s magnitude colours, r^s-luminosity (in Watts) and SFR(Hα) (equation 2), only accepting spaxels with SFR s/n >2 (leaving 48 273 spaxels in total). These data formed the ACC (see Fig. 7).

With the ACC constructed, for each galaxy it is possible to compare the SFR(Hα) map to its SFR(ACC) map. A galaxy's

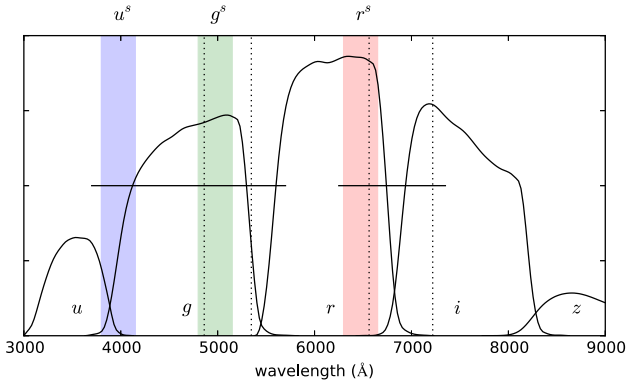

Figure 6. The custom filter set used to create the SAMI version of the aperture correction cube (ACC). The horizontal lines show the wavelength range of SAMI (blue and red arms of the AAOmega spectrograph). The vertical dotted lines show the limits of the locations of Hβ and Hα for $0 < z < 0.1$. The blue, green and red shaded areas represent the wavelength coverage of the custom SAMI filter-set, labelled as u^s, g^s, andr^s, respectively. The wavelength ranges of each filter are: 3800 Å $< u^s <$ 4150 Å, 4800 Å $< g^s <$ 5150 Å, and 6300 Å $< r^s <$ 6650 Å. The SDSS *u*, *g*, *r*, *i*, *z* filters are also overlaid for comparison. The SAMI filter set was required because the SAMI data does not span the full SDSS *g*, *r*, *i* filter range, due to the red arm of SAMI having over double the spectral resolution of the blue arm.

SFR(ACC) map is made by locating the u^s, g^s, r^s colours of a spaxel on the $u^s - g^s$ –, $g^s - r^s$ grid of the ACC and multiplying the SFR/r^s-band luminosity likelihood distribution of that cell by the spaxel's r^s-band luminosity. The SFR is taken as the median of the likelihood distribution. Regardless of the spatial distribution of the SFR(Hα), the SFR(ACC) followed a smooth distribution tracing out the optical continuum. This discontinuity is enhanced for more complex SFR(Hα) distributions (see Fig. 8 for a selection of these maps).

The second assumption from B04 that we can examine is that an aperture correction cube built from nuclear spectra can be representative of the SFR in the disc of a galaxy. Here, we proceed to build two ACCs in the same fashion as before, though this time with: (1) only spaxels contained in the central 3 arcsec diameter of the galaxy (nuclear); (2) only spaxels outside the central 3 arcsec (disc). These ACCs can be seen in Fig. 9. The most obvious difference is that the disc ACC spans a larger range of colours, but doesn't probe as far into $u^s - g^s$ as the nucleus ACC. This is expected as the nuclear region of galaxies tend to have redder colours due to the presence of older stars. Another difference arises in the likelihood distributions, with the medians of the nuclear ACC changing more rapidly than the disc ACC in the $u^s - g^s$, $g^s - r^s$ plane. This difference can be seen more easily in Fig. 10, where the data points are $u^s - g^s$, $g^s - r^s$ cells that overlap between the nuclear ACC and the disc ACC. A positive correlation is found between the difference of the likelihood-distribution medians for each ACC and the respective median Balmer decrements for a given $u^s - g^s$, $g^s - r^s$ cell. When the nuclear spectra underestimate the Balmer decrement for the disc, the SFR derived from an aperture correction cube built from only nuclear spectra is overestimated. Inversely, when the nuclear spectra overestimate the Balmer decrement for the disc, the SFR is underestimated. The histogram of the differences has a median value of 0.04 dex (underestimation of SFR) and a 1σ scatter of 0.16 dex. Whilst examining the effect of this correlation on the B04 against SAMI SFRs in Fig. 3, we also found a positive correlation between the total SFR of a galaxy and the ratio of median

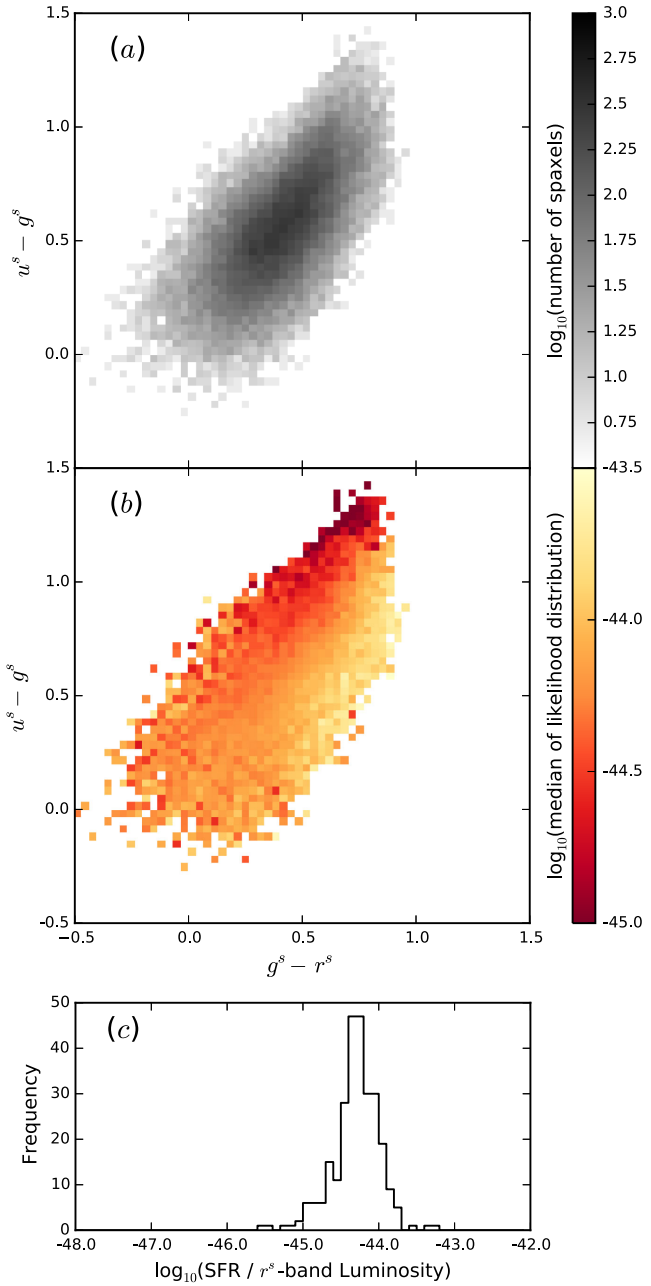

Figure 7. The SAMI version of the aperture correction cube (ACC), built from 48 273 spaxels. (a) shows the grid of $u^s - g^s$ versus $g^s - r^s$, with the intensity being the log$_{10}$(number of spaxels) that contribute to each cell. Each cell is 0.04 mag square in size. (b) is the same as (a), but the intensity is the log$_{10}$(median of the SFR/r^s-band luminosity likelihood distribution) for each cell. (c) is an example of the likelihood-distribution at the nominal point where $u^s - g^s = 0.5$, $g^s - r^s = 0.5$. Three hundred and twenty two spaxels contribute to this likelihood distribution, which has a median of −44.3 and a 1σ error of 0.35 dex.

Balmer decrement for spaxels within a 3 arcsec diameter aperture (nuclear) to the median Balmer decrement for remaining spaxels (disc; see Fig. 11).The spaxels that contributed to both ACCs occupied the same SF sequence on a log$_{10}$([O III] λ5007/Hβ) versus log$_{10}$([N II] λ6583/Hα) BPT diagram, ruling out contamination of other ionization sources to the nuclear spectra.

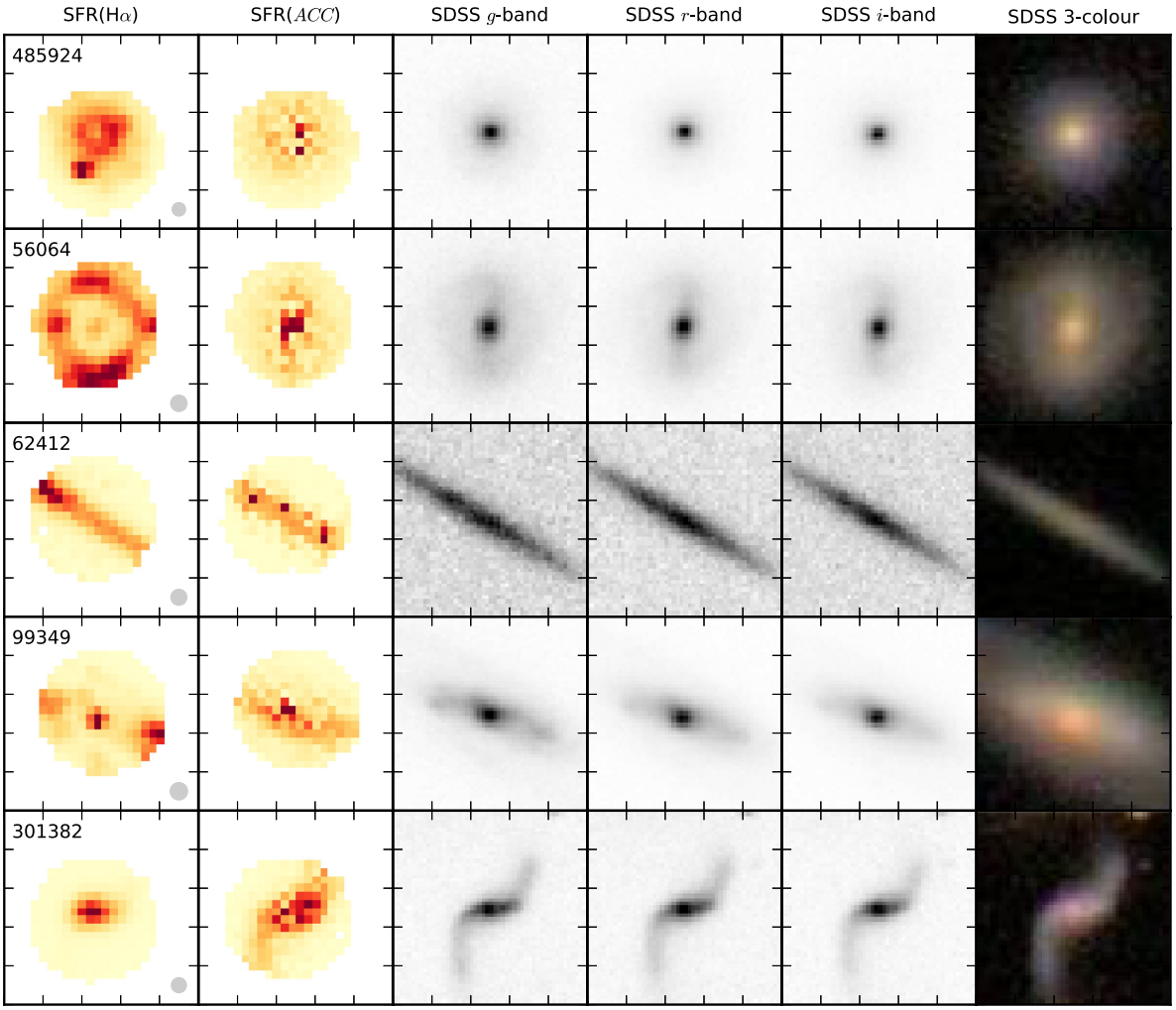

Figure 8. The SFR(Hα) map, SFR(ACC) map, SDSS g, r, i-band images and the SDSS three-colour image for five galaxies (a galaxy per row). Both SFR maps have been normalized to the maximum of each map, respectively. The g-band PSF size for the SAMI data is shown by a grey circle in the lower right of the SFR(Hα) maps. The SFR maps are made using SAMI cubes that have been binned to have 1 arcsec spaxels (native spaxel size is 0.5 arcsec). All maps and images are 25 $\times$ 25 arcsec in size, and are orientated such that north is up and east is left. The SAMI galaxy ID is provided in the upper left of the SFR(Hα) maps for reference in the text. These galaxies have been selected to highlight differences between the SFR maps. Only a few galaxies not represented here have smooth SFR maps that closely match each other.

4 DISCUSSION

4.1 H03 method (GAMA)

The attempt of disentangling random and systematic errors from SFR comparison plots, such as Fig. 3, can prove to be difficult, if not impossible. When comparing H03 SFRs and SAMI SFRs we find a near 1:1 trend (gradient of 0.91 $\pm$ 0.05 with a 1σ scatter of 0.22 dex). Deviation from 1:1 happens for low-SF galaxies, with H03 overpredicting the SFR. Studies of dwarf galaxies in the local Universe (which occupy the low-SF end of the H03 against SAMI SFRs in Fig. 3) have been shown to exhibit bursty star formation, in addition to an underlying ageing population (Gil de Paz, Madore & Pevunova 2003; Richards et al. 2014). An order of magnitude in the difference of time-scales leads to an r-band continuum level over-representing the instantaneous (Hα) star formation. The large scatter can be understood with the analysis of the SFR curves of growth (see Fig. 5), where galaxies with a small aperture ($d/R_{2P} < 0.4$) have an uncertainty on their aperture-corrected SFR $\approx$0.25 dex. The high dispersion of the H03 curves of growth at small apertures can also be seen in the work of Iglesias-Páramo et al. (2013) who at small apertures find large dispersions in the EW(Hα) and Balmer decrement profiles of 107 CALIFA galaxies with SFRs $\gtrsim$1 $M_\odot$ yr^{-1}. Finding no correlation between the H03 curves of growth and another global galaxy parameter results in an interpretation that the H03 error (Table 1) is random. The trend in the medians of these distributions, however, suggests that H03 are systematically overestimating their SFRs by up to 0.1 dex for galaxies with the smallest apertures ($d/R_{2P} < 0.2$). The analytical expressions of these error distributions (Table 1) can be used, together with measurement errors of the EW(Hα) and Balmer decrement, to obtain formal errors on the H03 SFRs.

The random nature of the H03 error should only be considered to be valid with an unbiased sample selection. Adopting a sample selection that could bias the EW(Hα) curves of growth will also introduce biases in the H03 SFRs. Such science can include investigation into the trends in SFR for merging galaxies, as star formation is seen to be more centrally concentrated in these systems, which

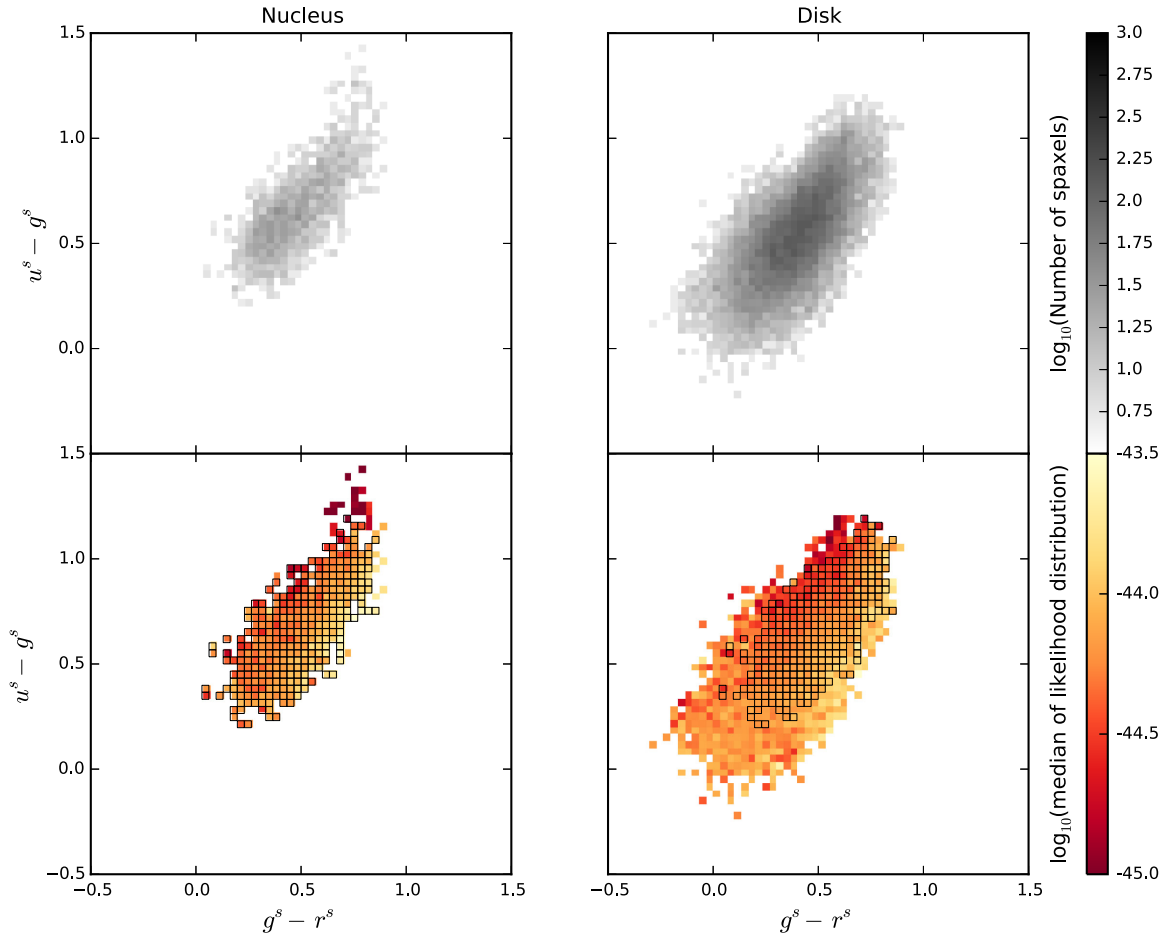

Figure 9. Two aperture correction cubes (ACC); one built from only spaxels in the central 3 arcsec of the galaxy (nucleus, left-hand column), and the other built from spaxels outside the central 3 arcsec (disc, right-hand column). The diagrams follow the same description as Fig. 7. Cells common between both ACCs are outlined in the lower panels. The disc ACC covers a larger range of colours (although, missing the reddest of spaxels with high $u^s - g^s$).

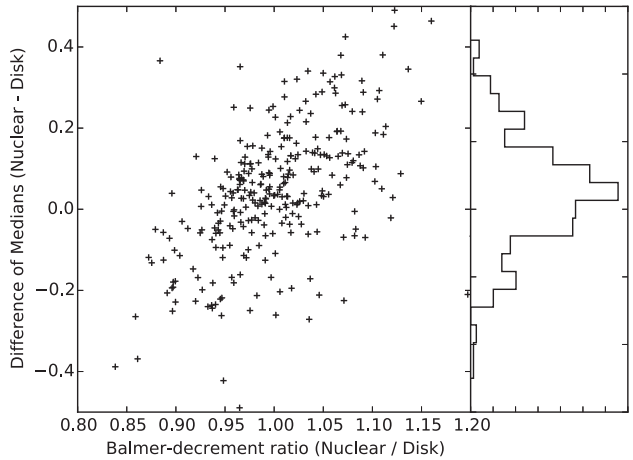

Figure 10. The difference of the median of the likelihood distributions (in dex) against the ratio of the median Balmer decrement for each common $u^s - g^s$, $g^s - r^s$ cell in the aperture correction cubes (nuclear ACC and the disc ACC, see Fig. 9). The Spearman's rank correlation coefficient is 0.561 with a p-value of 1.68×10^{-23}. The histogram shows the distribution of the differences, which has a median of 0.04 dex and a 1σ error of 0.16 dex. For positive difference the nuclear ACC underpredicts the SFR found from the disc ACC, and vice versa.

will lead to an overestimation of the H03 SFRs (Moreno et al. 2015, Bloom et al. *in prep*). Galaxies with centrally concentrated star formation are also more likely to be found in higher density environments (Koopmann, Haynes & Catinella 2006; Cortese et al. 2012, Schaefer et al. *in prep*), where the H03 SFRs would also become overestimated, although in this work we found no statistically significant correlation between the H03 SFR curves of growth and environment.

For GAMA DR2 galaxies with $z < 0.1$, the median $d/R_{2P} \approx 0.3$ and H03 1σ error $\approx$0.18 dex. Results such as the Hα luminosity function presented by Gunawardhana et al. (2013) will be affected by this error. The overestimation bias of up to 0.1 dex for apertures with $d/R_{2P} < 0.2$ can lead to a steeper turn-off in the shape of the Hα luminosity function at the high luminosity end (Gunawardhana, private communication). This section of the Hα luminosity function is where you tend to find larger galaxies (higher Hα luminosity), so the d/R_{2P} aperture size would be smaller.

4.2 B04 method (SDSS)

Understanding the slope of the B04 SFRs and SAMI SFRs from Fig. 3 required the creation of an aperture correction cube based on SAMI data (ACC) to discover how well broad-band colours could trace the Hα based star formation. Fig. 8 shows the SFR distributions of a selection of galaxies with SFR maps measured

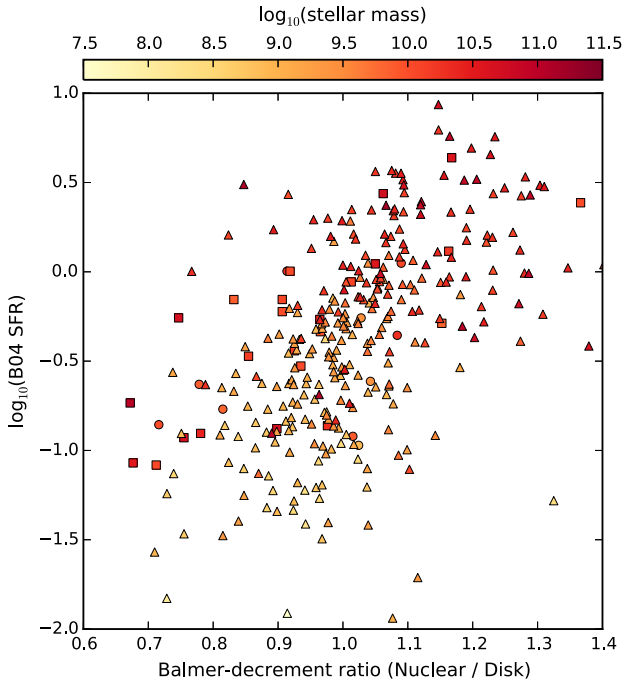

Figure 11. The $\log_{10}$(B04 SFRs) for 337 star-forming (SF) SAMI galaxies against the ratio of the median Balmer decrement for spaxels within a 3 arcsec aperture (nuclear) to the median Balmer decrement for spaxels outside a 3 arcsec aperture (disc). Square, triangle and circle markers represent early-type, late-type and unclassified morphologies, respectively, and are coloured with respect to each galaxy's stellar mass. The Spearman's rank correlation coefficient is 0.595 with a p-value of 1.46×10^{-26}. Galaxies with a higher SFR (or higher stellar mass) tend to have more dust in their disc compared to their nucleus.

from Hα and the ACC. Here we find that the SFR(ACC) traces out the broad-band light of the galaxy even when the SFR(Hα) is more clumpy. Clear examples of this from Fig. 8 are SAMI IDs 485924 and 56064. 485924 has an off-centre starburst which is not detected in the broad-band imaging or in the SFR(ACC). 56064 appears to have most of its star formation in the disc, but the SFR(ACC) predicts more star formation in the nucleus. Similarly to the analysis of H03 (see Fig. 4), only $\sim$1/3 of our galaxies exhibit a smooth distribution of SFR(Hα) that closely matches the distribution of SFR(ACC). Making SFR maps is not what the B04 aperture correction was intended for, although it highlights the need for IFS surveys of many thousands of galaxies.

In an aperture correction cube there is a degeneracy between stellar age, metallicity and dust that broadens the likelihood distributions, though the underlying issue is assuming the optical continuum (time-scales of $>$100 Myr) can trace SFR on time-scales $<$10 Myr. The effect of not being sensitive to starbursts can be one explanation to the underestimation in B04 SFRs for galaxies with a high SFR in Fig. 3. Although these galaxies are more likely to have bluer colours, they also have a tendency to have more prominent starbursts, resulting in the underestimation of B04 SFR. This underestimation has also been seen by Green et al., in preparation, who compare the B04 SFRs with total Hα SFRs from IFU data of 67 galaxies with SFRs of 1–100 $M_\odot$ yr^{-1}. Salim et al. (2007) found that for galaxies with B04 SFR of 1–30 $M_\odot$ yr^{-1}, the SFRs matched with SFRs derived from *FUV*, *NUV*, *u*, *g*, *r*, *i*, *z* broad-band measurements. This match is expected because the two star formation measures probe similar time-scales.

Fig. 9 shows a difference in the medians of the likelihood distributions of the nuclear ACC and disc ACC, meaning that the assumption in the B04 method that an ACC built from nuclear spectra can be representative of the galaxy as a whole has underlying errors. Investigating this difference further, we find a positive correlation between the medians of the likelihood distributions and the medians of the Balmer decrements for $u^s - g^s$, $g^s - r^s$ cells that are common between both ACCs (see Fig. 10). This is a probe into the degeneracy of dust in an aperture correction cube. Galaxies with strong increasing or decreasing dust gradients will have over- or underpredicted B04 SFRs, respectively. The dust gradient of a galaxy correlates with its total SFR (or stellar mass, see Fig. 11), such that high SF galaxies (or greater stellar mass) tend to have decreasing dust gradients, and low-SF galaxies have increasing dust gradients. Iglesias-Páramo et al. (2013) also find that galaxies with SFRs $\gtrsim$1 $M_\odot$ yr^{-1} have a decreasing dust gradient. This correlation might explain the slope in the B04 against SAMI SFRs from Fig. 3. The B04 SFRs for high SF galaxies are underpredicted compared to SAMI. This underrepresentation arises when deriving SFRs from an aperture correction cube that is built only using nuclear spectra. B04 also overpredict the SFR for low-SF galaxies for the same reason.

The B04 slope from Fig. 3 requires a correction term based on these correlations. However, due to the difference in broad-band filters used in B04 and this work to create the aperture correction cubes, we are unable to provide this correction. To find the true correction term, nuclear and disc aperture correction cubes would need to be built from IFS data of $\sim 10^3$ galaxies that spectrally cover the *g*, *r*, *i* filters. This will be possible with MaNGA or HECTOR (Lawrence et al. 2012; Bland-Hawthorn 2015). With these larger surveys, it will also be possible to investigate any biases that arise in the B04 method due to stellar age and metallicity.

In the age of multiwavelength surveys such as GAMA (Liske et al. 2015), analogous aperture correction cubes can be built from many different SFR indicators, and comparisons made to further identify possible biases. Any tracer of SFR can be used in the construction of an aperture correction cube, though the cube would be sensitive to different time-scales of star formation.

5 CONCLUSIONS

We have used IFS of 1212 galaxies from the SAMI Galaxy Survey to probe the assumptions that underpin the Hα SFR aperture correction methods of H03 and B04. We summarize the findings of this work:

(i) When comparing total SFRs from the H03 and B04 aperture corrections with integrated Hα SFRs from SAMI data, both H03 and B04 have trends that deviate from 1:1. The gradient and scatter for H03/SAMI are 0.91 $\pm$ 0.05 and 0.22 dex, and for B04/SAMI are 0.85 $\pm$ 0.03 and 0.15 dex.

(ii) Only $\approx$1/3 of our galaxies follow H03's assumption that the EW(Hα) and Balmer decrement curves of growth remain flat. For the sample considered here, the likelihood of increasing or decreasing curves of growth is the same. Our empirically derived, analytical expression of the error on and correction for this assumption can be found in Table 1. Using it, the median GAMA DR2 galaxy with redshift $z < 0.1$ has an H03 SFR 1σ error of 0.18 dex (not inclusive of measurement errors on EW(Hα) and Balmer decrement).

(iii) Investigations into the B04 method showed that although this method includes a dependence on optical colours, and is therefore more sensitive to younger, hotter stars, the SFRs found can still be insensitive to starbursts (instantaneous star formation). This is

because the Hα emission and optical continuum probe two different time-scales ($<$10 and $>$100 Myr, respectively).

(iv) We compared two aperture corrections similar to B04 from SAMI data, built from spectra of the nuclear regions of galaxies and separately from spectra beyond. We found B04's assumption that nuclear spectra can be representative of the rest of the galaxy to be biased due to a difference in the nuclear and disc dust corrections.

(v) We find that the dust gradient and total SFR of a galaxy are correlated such that galaxies with a high SFR require a smaller dust correction in their disc compared to their nucleus. This results in an underestimation of the total SFR when using a B04 aperture correction method built only from nuclear spectra. This bias is also seen in low-SF galaxies requiring a larger dust correction in their disc compared to their nucleus, resulting in an overestimation in SFR. The slope found when comparing total SFRs of SF galaxies from B04 and SAMI can be explained by these correlations.

(vi) Measuring the magnitude of the bias in the B04 aperture correction requires further investigation using IFS data that covers the same wavebands (e. g. MaNGA or HECTOR).

(vii) A sample selection that prefers galaxies with concentrated or extended star formation will bias the H03 SFRs to be over- or underestimated, respectively. Whereas, a sample selection that prefers galaxies with high or low star formation will bias the B04 SFRs. Choosing which aperture correction is suitable to minimize any potential bias will depend on the data sample in question.

So, 'Can we trust aperture corrections to predict star formation?' Yes, but only for large ($\gtrsim 10^3$) unbiased samples of galaxies, and as long as the conclusions can have accuracies of $\sim$0.2 dex in SFR. At this level of uncertainty, there are two main cases of preference between the H03 and B04 aperture correction methods: (a) the inclusion of galaxies classified outside of the star formation main sequence in BPT diagnostics is only possible in the B04 method; (b) the H03 method has lower systematic biases over a large dynamic range in SFR for complete data samples.

ACKNOWLEDGEMENTS

The SAMI Galaxy Survey is based on observation made at the Anglo-Australian Telescope. The Sydney-AAO Multi-object Integral field spectrograph (SAMI) was developed jointly by the University of Sydney and the Australian Astronomical Observatory. The SAMI input catalogue is based on data taken from the Sloan Digital Sky Survey, the GAMA Survey and the VST ATLAS Survey. The SAMI Galaxy Survey is funded by the Australian Research Council Centre of Excellence for All-sky Astrophysics (CAASTRO), through project number CE110001020, and other participating institutions. The SAMI Galaxy Survey website is http://sami-survey.org/.

The ARC Centre of Excellence for All-sky Astrophysics (CAASTRO) is a collaboration between The University of Sydney, The Australian National University, The University of Melbourne, Swinburne University of Technology, The University of Queensland, The University of Western Australia and Curtin University, the latter two participating together as the International Centre for Radio Astronomy Research (ICRAR). CAASTRO is funded under the Australian Research Council (ARC) Centre of Excellence program, with additional funding from the seven participating universities and from the NSW State Government's Science Leveraging Fund.

Funding for SDSS-III has been provided by the Alfred P. Sloan Foundation, the Participating Institutions, the National Science Foundation, and the U.S. Department of Energy Office of Science. The SDSS-III web site is http://www.sdss3.org/.

GAMA is a joint European-Australasian project based around a spectroscopic campaign using the Anglo-Australian Telescope. The GAMA website is http://www.gama-survey.org/.

SMC acknowledges support from an ARC Future fellowship (FT100100457). JTA acknowledges the award of an ARC Super Science Fellowship (FS110200013). MSO acknowledges the funding support from the Australian Research Council through a Future Fellowship (FT140100255) MLPG acknowledges support from a European Research Council grant (DEGAS-259586). LC acknowledges support under the Australian Research Council's Discovery Project funding scheme (DP130100664).

REFERENCES

Abazajian K. N. et al., 2009, ApJS, 182, 543
Ahn C. P. et al., 2014, ApJS, 211, 17
Allen J. T. et al., 2015, MNRAS, 446, 1567
Baldwin J. A., Phillips M. M., Terlevich R., 1981, PASP, 93, 5
Bland-Hawthorn J., 2015, in Ziegler B. L., Combes F., Dannerbauer H., Verdugo M., eds, Proc. IAU Symp. 309, Galaxies in 3D across the Universe. Cambridge Univ. Press, Cambridge, p 21
Bland-Hawthorn J. et al., 2011, Opt. Express, 19, 2649
Brinchmann J., Charlot S., White S. D. M., Tremonti C., Kauffmann G., Heckman T., Brinkmann J., 2004, MNRAS, 351, 1151 (B04)
Brough S. et al., 2013, MNRAS, 435, 2903
Bryant J. J., Bland-Hawthorn J., Fogarty L. M. R., Lawrence J. S., Croom S. M., 2014, MNRAS, 438, 869
Bryant J. J. et al., 2015, MNRAS, 447, 2857
Bundy K. et al., 2015, ApJ, 798, 7
Calzetti D., 2001, PASP, 113, 1449
Calzetti D., Kennicutt R. C., 2009, PASP, 121, 937
Cappellari M., Emsellem E., 2004, PASP, 116, 138
Cardelli J. A., Clayton G. C., Mathis J. S., 1989, ApJ, 345, 245
Charlot S., Longhetti M., 2001, MNRAS, 323, 887
Cluver M. E. et al., 2014, ApJ, 782, 90
Cortese L. et al., 2012, A&A, 544, A101
Cortese L. et al., 2014, ApJ, 795, L37
Croom S. M. et al., 2012, MNRAS, 421, 872
Dopita M. A., Sutherland R. S., 2003, Astrophysics of the Diffuse Universe. Springer, Berlin, New York
Driver S. P. et al., 2009, Astron. Geophys., 50, 12
Drory N. et al., 2015, AJ, 149, 77
Falcón-Barroso J., Sánchez-Blázquez P., Vazdekis A., Ricciardelli E., Cardiel N., Cenarro A. J., Gorgas J., Peletier R. F., 2011, A&A, 532, A95
Gerssen J., Wilman D. J., Christensen L., 2012, MNRAS, 420, 197
Gil de Paz A., Madore B. F., Pevunova O., 2003, ApJS, 147, 29
Gunawardhana M. L. P. et al., 2013, MNRAS, 433, 2764
Ho I.-T. et al., 2014, MNRAS, 444, 3894
Hopkins A. M. et al., 2003, ApJ, 599, 971 (H03)
Hopkins A. M. et al., 2013, MNRAS, 430, 2047
Iglesias-Páramo J. et al., 2013, A&A, 553, L7
Jansen R. A., Franx M., Fabricant D., Caldwell N., 2000a, ApJS, 126, 271
Jansen R. A., Fabricant D., Franx M., Caldwell N., 2000b, ApJS, 126, 331
Kauffmann G. et al., 2003, MNRAS, 346, 1055
Kelvin L. S. et al., 2012, MNRAS, 421, 1007
Kelvin L. S. et al., 2014, MNRAS, 444, 1647
Kennicutt,Jr R. C., 1998, ApJ, 498, 541
Kewley L. J., Jansen R. A., Geller M. J., 2005, PASP, 117, 227
Koopmann R. A., Haynes M. P., Catinella B., 2006, AJ, 131, 716
Lawrence J. et al., 2012, Proc. SPIE, 8446, 844653
Le Fèvre O. et al., 2003, in Iye M., Moorwood A. F. M., (eds), Proc. SPIE, 4841, 1670
Liske J. et al., 2015, MNRAS, 452, 2087

Markwardt C. B., 2009, in Bohlender D. A., Durand D., Dowler P., eds, ASP Conf. Ser. Vol. 411, Astronomical Data Analysis Software and Systems XVIII. Astron. Soc. Pac., San Francisco, p. 251
Moreno J., Torrey P., Ellison S. L., Patton D. R., Bluck A. F. L., Bansal G., Hernquist L., 2015, MNRAS, 448, 1107
Richards S. N. et al., 2014, MNRAS, 445, 1104
Salim S. et al., 2007, ApJS, 173, 267
Salpeter E. E., 1955, ApJ, 121, 161
Sánchez S. F. et al., 2012, A&A, 538, A8
Sharp R. et al., 2006, in Society of Photo-Optical Instrumentation Engineers (SPIE) Conference Series, Vol. 6269, p. 0
Sharp R. et al., 2015, MNRAS, 446, 1551
Sharples R. et al., 2006, New Astron. Rev., 50, 370
Sharples R. et al., 2013, Messenger, 151, 21
Taylor E. N. et al., 2011, MNRAS, 418, 1587
York D. G. et al., 2000, AJ, 120, 1579

This paper has been typeset from a TEX/LATEX file prepared by the author.